Photochemical & Photobiological Sciences (2023) 22:1561–1572
https://doi.org/10.1007/s43630-023-00397-2

ORIGINAL PAPERS

The organization of the phycobilisome-photosystem I supercomplex depends on the ratio between two different phycobilisome linker proteins

Mai Watanabe[1,2,3] · **Masahiko Ikeuchi**[2] · **Annegret Wilde**[1]

Received: 23 November 2022 / Accepted: 16 February 2023 / Published online: 1 March 2023

Abstract

The phycobilisome (PBS) is an antenna protein complex in cyanobacteria, Glaucocystophytes, and red algae. In the standard PBS, the rod-core PBS, the rods are connected to the core by the rod-core linker protein CpcG. The rod-core PBS transfers the light energy mainly to photosystem (PS) II and to a lesser extent to PSI. Cyanobacteria assemble another type of PBS, the CpcL-PBS, which consists of only one rod. This rod-type PBS is connected to the thylakoid membrane by the linker protein CpcL and is a PSI-specific antenna. In the filamentous heterocyst-forming cyanobacterium *Anabaena* (*Nostoc*) sp. PCC 7120, the CpcL-PBS forms a complex with the tetrameric PSI (PBS-PSI supercomplex). The CpcL-PBS and the rod part of the rod-core PBS are identical except for the linker proteins CpcL and CpcG. How cells control the accumulation of the two different types of PBS is unknown. Here, we analyzed two mutant strains which either lack the major rod-core linker CpcG4 or overexpress the rod-membrane linker CpcL. In both mutant strains, more and larger PBS-PSI supercomplexes accumulated compared to the wild type. Our results suggest that CpcL and CpcG4 compete for the same phycobiliprotein pool, and therefore the CpcL/CpcG4 ratio determines the levels of PBS-PSI supercomplexes. We propose that the CpcL-PBS and the rod-core PBS fulfill distinct functions in light harvesting.

Graphical abstract

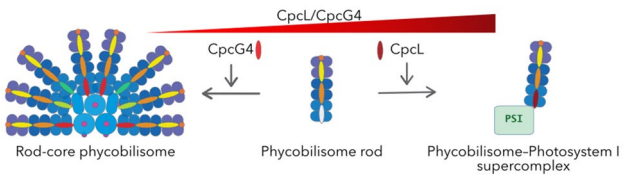

Keywords Phycobilisome · CpcL-phycobilisome · Photosystem I-specific antenna · Linker protein

This publication is dedicated to Prof. Silvia E. Braslavsky, a pioneer in photobiology and photobiophysics, on the occasion of her 80th birthday.

✉ Mai Watanabe
mai.watanabe@biologie.uni-freiburg.de;
maiwatanabe.ps@gmail.com

[1] Faculty of Biology, Institute of Biology III, University of Freiburg, 79104 Freiburg, Germany

[2] Department of Life Sciences (Biology), Graduate School of Arts and Sciences, University of Tokyo, Komaba, Meguro, Tokyo 153-8902, Japan

[3] Present Address: Department of Biological Sciences, Graduate School of Science, Tokyo Metropolitan University, Minami-Ohsawa, Hachioji, Tokyo 192-0397, Japan

1 Introduction

Light serves as an essential energy source for life on earth. Photosynthesis enables the conversion of light energy into chemical energy to support almost all biological processes in a phototrophic cell. Light-harvesting antenna systems which efficiently collect the light energy are crucial components of the photosynthetic apparatus. Many cyanobacteria, Glaucocystophytes, and red algae use phycobilisomes (PBSs) as light-harvesting antenna complexes. The PBS absorbs light and transfers the excitation energy to the photosystem (PS) complexes, mainly to PSII [1]. Generally, the

PBS is a supercomplex composed of a core and protruding rod subcomplexes (the rod-core PBS). These core and rod subcomplexes are composed of various phycobilin-binding proteins connected by several classes of colorless linker proteins [2, 3]. The phycobiliproteins can be classified into allophycocyanin (APC, λ_{max} = 650–655 nm) which forms the core, phycocyanin (PC, λ_{max} = 620 nm) which is the main component of the rod, phycoerythrin (PE), and phycoerythrocyanin (PEC), both of which can be assembled into the peripheral part of the rods in different species [4, 5]. The rod-core linker protein CpcG connects the rods to the core complex and is necessary for the assembly of the rod-core PBS [3]. In general, CpcG proteins contain a conserved N-terminal linker-PBS domain (Pfam00427), located within the rod disc, and a C-terminal hydrophilic linker-G domain, which interacts with the core [3, 6]. The chromosome of the filamentous, N_2-fixing cyanobacterium *Anabaena* (*Nostoc*) sp. PCC 7120 (hereafter "*Anabaena*") contains three copies of the rod-core linker CpcG which are designated as CpcG1, CpcG2, and CpcG4. It is known that CpcG4 is the rod-core linker that makes the connection between rods and the central core cylinders of the PBS. CpcG1 and CpcG2 linker proteins connect the rods to the so-called half-core cylinders which are composed of only one APC hexamer (Fig. 1) [6]. These half-core cylinders are located perpendicularly on top of the two basal core cylinders in the *Anabaena* PBS.

Further, another type of PBS has been reported, which is called the CpcL-PBS [7–9]. The CpcL-PBS is a rod-type PBS composed of a single PBS rod and the rod-membrane linker CpcL. Previously, CpcL was called CpcG2 in *Synechocystis* sp. PCC 6803 and CpcG3 in *Anabaena*. In the following, we use only the name CpcL to designate the rod-membrane linker protein in different organisms. CpcL has an N-terminal linker-PBS domain, almost identical to that of the rod-core linker CpcG proteins, and a C-terminal hydrophobic linker-L domain [3, 9]. The hydrophobic linker-L domain enables the direct interaction of the rod with the thylakoid membrane [9]. While the rod-core PBS serves as a major antenna for PSII, CpcL-PBS mediates the energy transfer specifically to PSI [9–11]. The fast and efficient energy transfer from CpcL-PBS to PSI is comparable to that from the rod-core PBS to PSII [11].

In *Anabaena*, PSI forms a tetramer structure, which has been confirmed as the dimer-of-dimer in cryo-electron microscopy (cryo-EM) [12, 13]. The CpcL-PBS interacts with the PSI tetramer to form a PBS-PSI supercomplex [9]. The single-particle electron microscopy (EM) structure of the PBS-PSI supercomplex revealed that CpcL-PBS is attached to the interface between two monomers within the dimer of the PSI tetramer [9]. Theoretically, the dimer-of-dimer structure revealed two such binding sites within the dimers and two potential binding sites between the dimers. However, it is not yet elucidated whether more CpcL-PBS could bind to the PSI tetramer.

CpcL-PBS forms a PBS-PSI supercomplex and transfers the light energy to PSI. On the other hand, the rod-core PBS can also function as a PSI antenna. Here, we revealed the role of linker proteins on the amount of different PBS assemblies and supercomplexes. We characterized two deletion mutants lacking the linker genes for the rod-core PBS (Δ*cpcG4*) or the CpcL-PBS (Δ*cpcL*), and a *cpcL* overexpression mutant. Our results demonstrate that the linker proteins compete for the assembly of the corresponding PBS. In addition, the similarity of the PBS-PSI supercomplex assembly in the *cpcL* overexpression and Δ*cpcG4* mutants suggests that the CpcL/CpcG4 linker ratio determines the amount of PBS-PSI supercomplexes in the cell.

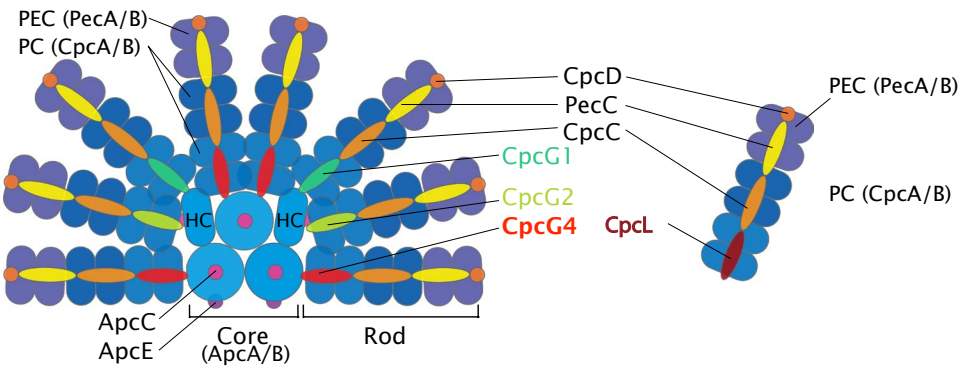

Fig. 1 Model of the rod-core PBS (left) and the CpcL-PBS (right) from *Anabaena*. The rod-core linker CpcG4 connects rods with core cylinders, whereas the CpcL rod-membrane linker connects a single rod with the thylakoid membrane. The additional rod-core linkers CpcG1 and CpcG2 connect rods with the half-core cylinder (HC) [6]. In the rod-core PBS, the linker ApcE connects the core with the membrane. *Anabaena* PBSs contain the phycobiliproteins phycoerythrocyanin (PEC), phycocyanin (PC), and allophycocyanin (APC) and additional linkers which connect the different structures

2 Materials and methods

2.1 Strains and growth conditions

Wild type and mutants of *Anabaena* sp. PCC 7120 were grown at 31 °C in liquid BG11 medium supplemented with 20 mM HEPES KOH (pH 8.2) [14] and with bubbling with 1% CO_2 under continuous illumination with white fluorescent lamps (ca. 20 µmol photons m^{-2} s^{-1}). For the cultivation of mutant strains, 30 µg mL^{-1} neomycin or 20 µg mL^{-1} erythromycin were added.

2.2 Construction of mutants

All primers are listed in Table S1. For the *cpcL* gene deletion, upstream, downstream-1, and downstream-2 regions of the *cpcL* gene were amplified by PCR using primer pairs of cpcG2-1F/cpcG2-2R, cpcG4-1F/cpcG4-2R, and all0538-1F/all0538-2R, respectively. Details of the construction of the plasmids are shown in Fig. 2A. PCR products of upstream and downstream-1 were subcloned into pPCRScript separately, and the downstream-2 fragment was subcloned into pT7Blue. The respective upstream and the downstream DNA fragments were digested with BamHI/EcoRI or ClaI/XhoI, respectively, and were ligated. The neomycin resistance cassette was inserted into the EcoRI site between the downstream-1 and 2 DNA fragments. The *cpcG4* gene was inactivated by the insertion of the neomycin resistance cassette into a HpaI site. The XhoI–SacI fragment from pPCRScript_Δ*cpcL*::Nm^R and pT7Blue_Δ*cpcG4*::Nm^R were subcloned into the *sacB*-vector pRL271 between the XhoI and SacI sites [15], resulting in pRL271_Δ*cpcL*::Nm^R (Δ*cpcL*) and pRL271_Δ*cpcG4*::Nm^R (Δ*cpcG4*). The overexpression plasmid for the *cpcL* gene was constructed as follows. The subcloned *cpcL* gene in the pPCRScript was digested by BglII and SalI and ligated into the BamHI/SalI digested pAM505-based shuttle vector [16, 17] pAM505::Er^R creating the pAM505::Er^R_*cpcL* plasmid. The pAM505::Er^R_*cpcL* and the *trc* promoter [18–20] were amplified by PCR using primer pairs cpcL-6F/pAM505-6R and trc-19FpAM505/trc-20RAncpcL and combined using the In-Fusion System (Takara).

Mutation of *Anabaena* was achieved by triparental conjugation using strain J53 bearing RP4 and cargo strain HB101, bearing the helper plasmid pRL623 [21]. The selection of double recombinants was performed using *sacB* as a negative selection marker [22]. The correct genome modification and the complete segregation of mutant alleles in Δ*cpcL* and Δ*cpcG4* mutants were verified by PCR using the primer pairs cpcG2-1F/cpcG4-2R, and cpcG4-1F/cpcG4-2R, respectively. Primer pair cpcL-4R/trc-19FpAM505 was used for PCR to verify the presence of the plasmid in the *cpcL* overexpression mutants.

2.3 Isolation of phycobilisomes

PBSs were isolated as previously described [9]. Briefly, cells were harvested, washed twice with 0.9 M potassium phosphate buffer (pH 7.0), and broken with zirconia beads with a bead beater (Micro Smash MS-100R; TOMY). The cell extract was treated with 2% (v/v) Triton X-100 in 0.9 M phosphate buffer (pH 7.0) for 30 min and centrifuged at 20,000×*g* for 20 min at 18 °C to separate the upper green Triton X-100 layer from the lower blue aqueous phase. The blue phase was loaded onto a 10–50% (w/v) linear sucrose density gradient with 0.9 M phosphate buffer and centrifuged at 130,000×*g* for 16 h at 18 °C.

2.4 Isolation of photosystem complexes

PS complexes were isolated as described in a previous report [9]. Cells were harvested, resuspended in buffer A containing 50 mM 4-morpholineethanesulfonic acid sodium hydroxide (pH 6.5), 10 mM $MgCl_2$, 5 mM $CaCl_2$, and 25% (w/v) glycerol, and disrupted with zirconia beads with a bead beater (Micro Smash MS-100R; TOMY). After removing unbroken cells, the resulting supernatant was centrifuged at 300,000×*g* for 30 min at 4 °C to separate thylakoid fractions and soluble proteins. Thylakoid fractions were adjusted to a concentration of 1 mg chlorophyll (Chl) mL^{-1} with buffer A and solubilized with 1% n-dodecyl-β-D-maltoside (DM) (Sigma-Aldrich) on ice for 30 min, followed by centrifugation at 300,000 × g for 30 min at 4 °C. The supernatant was diluted with three volumes of buffer B (50 mM 4-morpholineethanesulfonic acid sodium hydroxide (pH 6.5), 10 mM $MgCl_2$, and 5 mM $CaCl_2$), loaded onto a 10–30% linear sucrose density gradient in buffer B containing 0.01% DM, and centrifuged at 130,000×*g* for 6–8 h at 4 °C.

2.5 SDS-PAGE and Western blot analysis

Proteins were separated by SDS-urea-PAGE with a 16–22% (w/v) linear gradient of polyacrylamide containing 7.5 M urea [23], followed by Coomassie or silver staining [24]. The bilin fluorescence of the phycobiliproteins was detected through a 605 nm filter with excitation at 532 nm (FMBIO II, TaKaRa) before silver staining. Western blot analysis was performed as described before [9]. The peptide antibodies for CpcL, CpcG4, and CpcG1 were produced by Takara Bio and used for immunodetection.

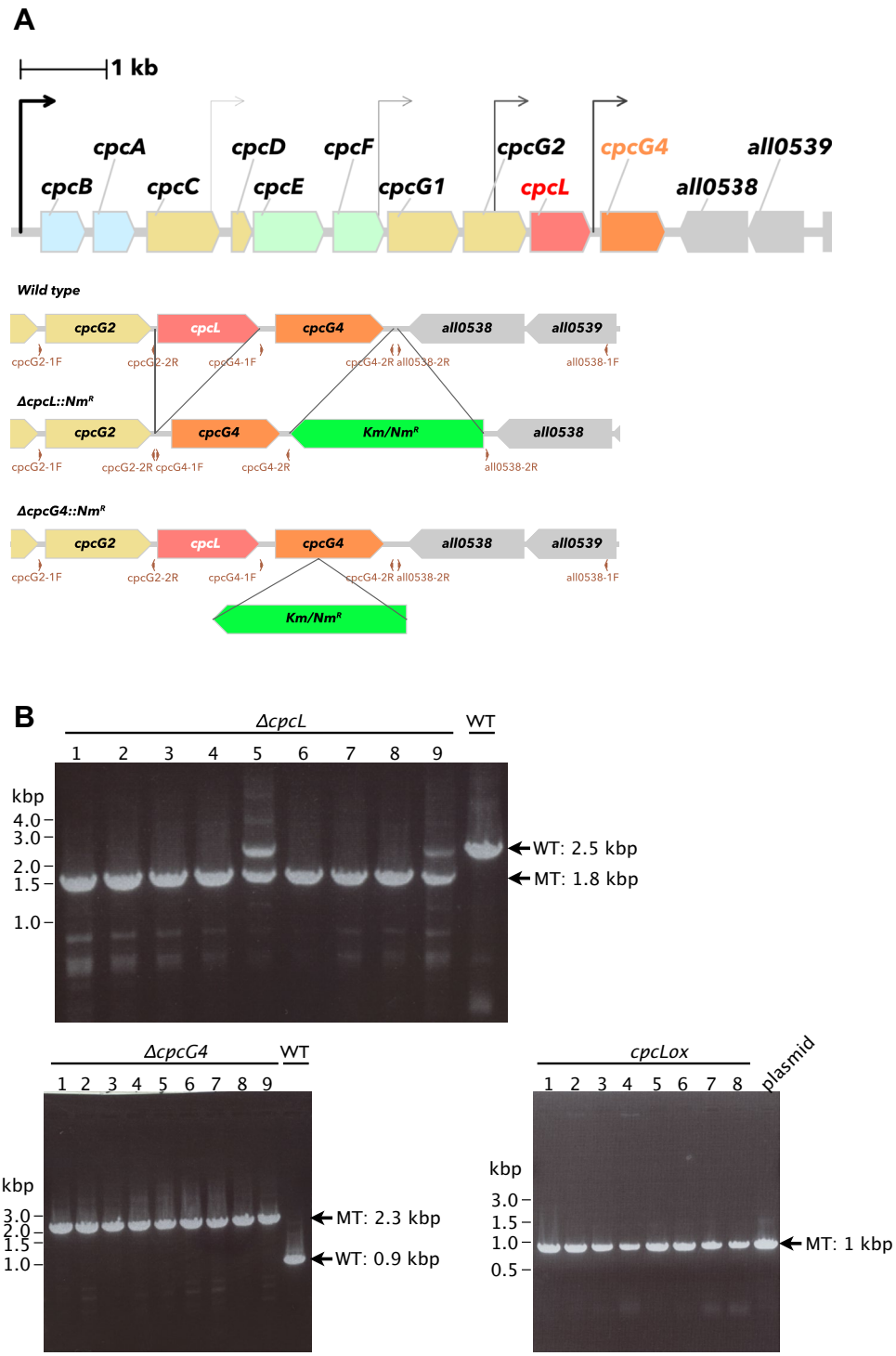

Fig. 2 **a** Scheme of the *cpc* operon in *Anabaena* and a map illustrating the construction of the Δ*cpcL* and Δ*cpcG4* mutants. The arrows show the putative transcription start sites as predicted by RNA-seq data [29]. For Δ*cpcL* mutant construction, to avoid polar effects on the downstream *cpcG4* gene expression, the complete ORF of the *cpcL* gene was deleted, and the kanamycin/neomycin resistance cassette was inserted into an intergenic region after the whole *cpc* operon. For Δ*cpcG4* construction, the kanamycin/neomycin resistance cassette was inserted into the *cpcG4* gene. **b** Verification of complete segregation of mutant alleles in Δ*cpcL* and Δ*cpcG4* mutants and presence of the *cpcL* overexpression plasmid by PCR. Wild type (WT) served as a negative control. Expected product sizes are 1755 bp or 2475 bp for Δ*cpcL* mutant and WT, 2281 bp or 931 bp for Δ*cpcG4* mutant or WT, and 982 bp for *cpcL* overexpression mutant. Clone 1 was used each time for the analyses in this study

2.6 Absorption and 77 K fluorescence spectroscopy

Absorption spectra were measured at room temperature (UV-2400PC; Shimadzu). Fluorescence excitation spectra were measured with a fluorescence spectrophotometer (RF-5300PC; Shimadzu) equipped with a Dewar vessel containing liquid nitrogen. Samples were excited from 400 to

700 nm and fluorescence was monitored at the PSI emission peak at 725 nm.

3 Results

3.1 Construction of *Anabaena* mutants lacking the linker proteins CpcL and CpcG4

In order to evaluate the assembly of PBS-PSI supercomplexes in the absence of CpcL and CpcG4, we constructed the respective mutant strains Δ*cpcL* and Δ*cpcG4*. In *Anabaena*, the *cpcL* gene locates upstream of *cpcG4* in an operon including genes encoding other PBS subunits (Fig. 2a). To avoid polar effects of a *cpcL* mutation on the downstream *cpcG4* gene expression, we deleted the complete ORF of the *cpcL* gene and inserted the neomycin resistance cassette into an intergenic region after the whole operon (Fig. 2a). We verified the correct genome modification and the complete segregation of mutant alleles in Δ*cpcL* and Δ*cpcG4* mutants by PCR (Fig. 2b), and used one completely segregated clone for further analyses. In addition to the gene deletion mutants, we also created a *cpcL* overexpression mutant in *Anabaena*. The *cpcL* gene was inserted together with a synthetic *trc* promoter into a self-replicating plasmid [20]. The presence of the plasmid in conjugated cells was verified by PCR (Fig. 2b).

3.2 Isolation of PBS fractions from Δ*cpcL* and Δ*cpcG4* mutants

To investigate the effects of the disruption of *cpcL* and *cpcG4* genes, we isolated PBSs by linear sucrose density gradient centrifugation from wild type, Δ*cpcL*, and Δ*cpcG4* mutants grown under standard conditions (Fig. 3a). Distributions of CpcL-PBS and the rod-core PBS in the gradients were analyzed by Western blot analysis using an anti-CpcL antibody for CpcL-PBS, anti-CpcG4, and anti-CpcG1 antibodies for the rod-core PBS, respectively (Fig. 3b). In the wild type, CpcL and CpcG4 were detected in fractions 2–10 and 5–10, respectively (Fig. 3b). Similarly to a previous study [9], we detected the rod-core PBSs in several fractions (Fig. 3a, b). Fraction 4 did not correspond to a clearly visible band but rather to a pale blue region in the sucrose gradient (Fig. 3a). This fraction mainly contained CpcL and did not show prominent APC absorption (650 nm) in the spectra (Fig. 3c), indicative of the presence of CpcL–PBS complexes only. In the Δ*cpcL* mutant, no colored region corresponding to fraction 4 of the wild type was observed, whereas the rod-core PBS fractions (fractions 5–10 in the wild type) are clearly visible in this mutant (Fig. 3a, fractions 15–19 in Δ*cpcL*). We took the non-colored region of the Δ*cpcL* gradient (fraction 14) and measured the absorption spectra. Fraction 14 showed almost no absorption (Fig. 3c). In the Δ*cpcG4* mutant, CpcL was detected in fractions 21–25 (Fig. 3b, lower panel). In the gradient, fraction 23 was at the same position as fraction 4 of wild type and was clearly colored (Fig. 3a). This fraction did not include the rod-core linker CpcG1 (Fig. 3b, lower panel). Absorption spectra revealed that fraction 23 includes PC and APC (Fig. 3c). These results suggest that this fraction is a mixture of the CpcL-PBS and detached discs from the rod-core PBS and that the assembly of CpcL-PBS was not affected in the Δ*cpcG4* mutant. These results confirm that CpcL is a specific linker of the CpcL-PBS. The rod-core linker CpcG1 was detected in fractions 24 and 25 of the Δ*cpcG4* mutant preparation, indicating that these two fractions contain the rod-core PBS (Fig. 3b). Absorption spectra showed a high APC-to-PC ratio in fractions 24 and 25, suggesting that these fractions contain a low amount of PBS rods (Fig. 3c). This result is consistent with previous analyses [6, 25], which showed that CpcG4 is the central rod-core linker in the rod-core PBS, and CpcG1 or CpcG2 cannot replace CpcG4.

3.3 Effect of *cpcL* deletion on PBS-PSI supercomplex formation

Next, we separated the PS complexes from the solubilized thylakoid fraction of the Δ*cpcL* mutant in sucrose gradients (Fig. 4a). In the Δ*cpcL* mutant, a green fraction which would correspond to the PBS-PSI supercomplex was not detected (fraction 4 of wild type). Therefore, we collected the fraction from the gradient of the Δ*cpcL* mutant which had a similar position in the gradient as the PBS-PSI in the wild type (fraction 4* in Fig. 4a) and performed SDS-PAGE and measured absorption spectra (Fig. 4b, c). Fraction 4* from the Δ*cpcL* mutant contained PSI, but no CpcL and PC subunits (Fig. 4b). The absorption spectrum confirmed that the fraction 4* did not contain PC (Fig. 4c). These results indicate that the CpcL linker is crucial for the PBS-PSI supercomplex assembly.

3.4 Isolation of PBS-PSI supercomplexes from a *cpcL* overexpression mutant

Overexpression of *cpcL* generated two blue-green bands (fractions 5 and 6), which appeared below the typical dense bands (fractions 3 and 4) in the gradient (Fig. 5a). We analyzed the subunit composition of the larger supercomplexes (fractions 5 and 6) by SDS-PAGE. Bilin fluorescence image and silver-staining demonstrated that they include PSI as well as PC subunits, which were nearly identical to the profile of fraction 4 (Fig. 5b). Absorption spectra confirmed the presence of PC in the fractions 5 and 6. Notably, the PC content of fraction 6 was prominent compared with fraction 5.

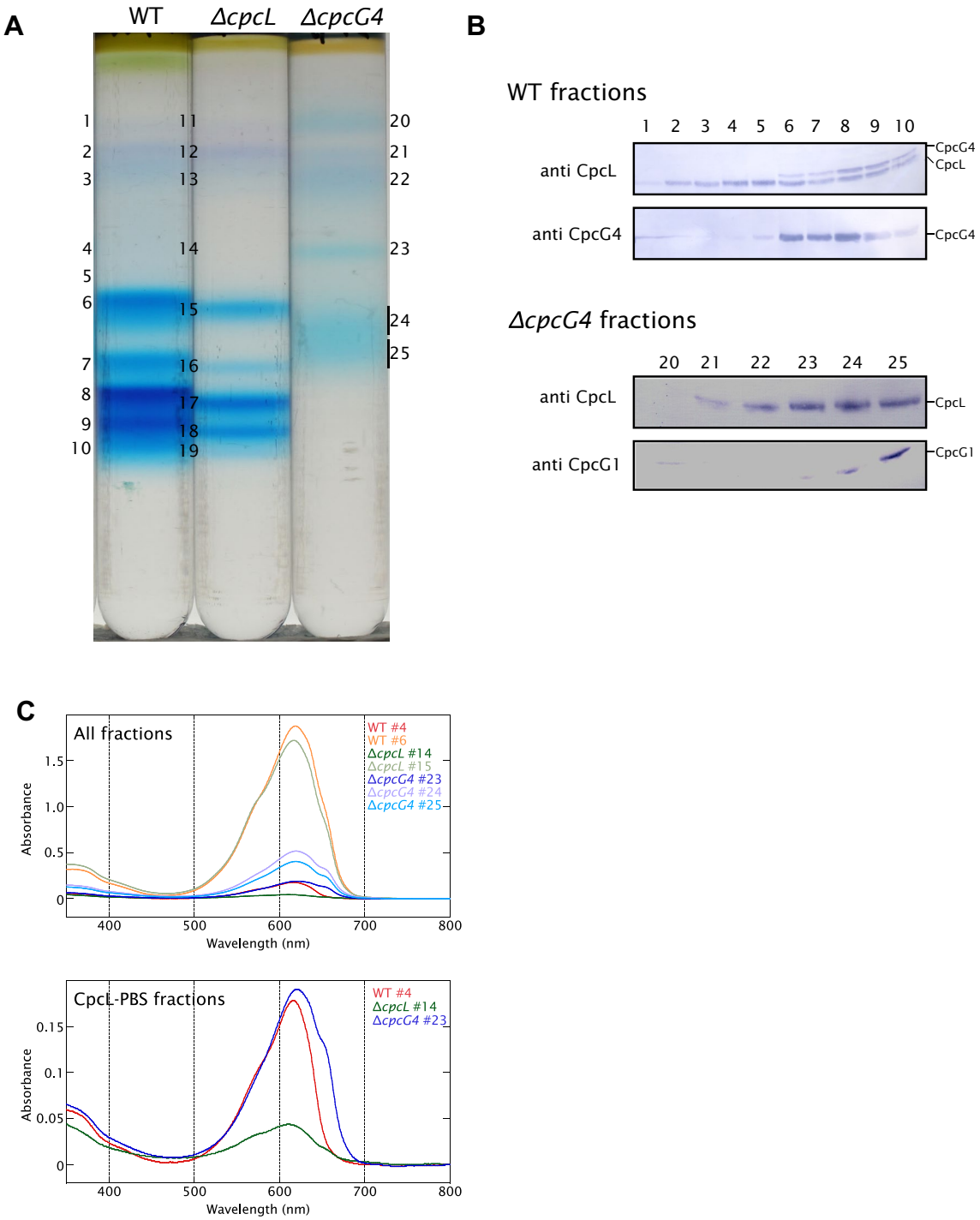

Fig. 3 Isolation of CpcL-PBSs and rod-core PBSs by centrifugation with a linear sucrose gradient under high-salt conditions. **a** Separation patterns of PBS fractions from wild type, Δ*cpcL*, and Δ*cpcG4* after centrifugation at 130,000×*g* for 18 h at 18 °C. (B) Western blot analysis of CpcL, CpcG4, and CpcG1 linker proteins with specific antibodies in the different fractions from wild type and the Δ*cpcG4* mutant. The same volume of samples was applied to the SDS-PAGE gel. Lane numbers correspond to the fractions numbered in (**a**). **c** Absorption spectra of PBS fractions from wild type and mutant samples. Fractions were directly used for the measurement without further dilution. Sample numbers correspond to the numbered fractions in (A). WT, wild type

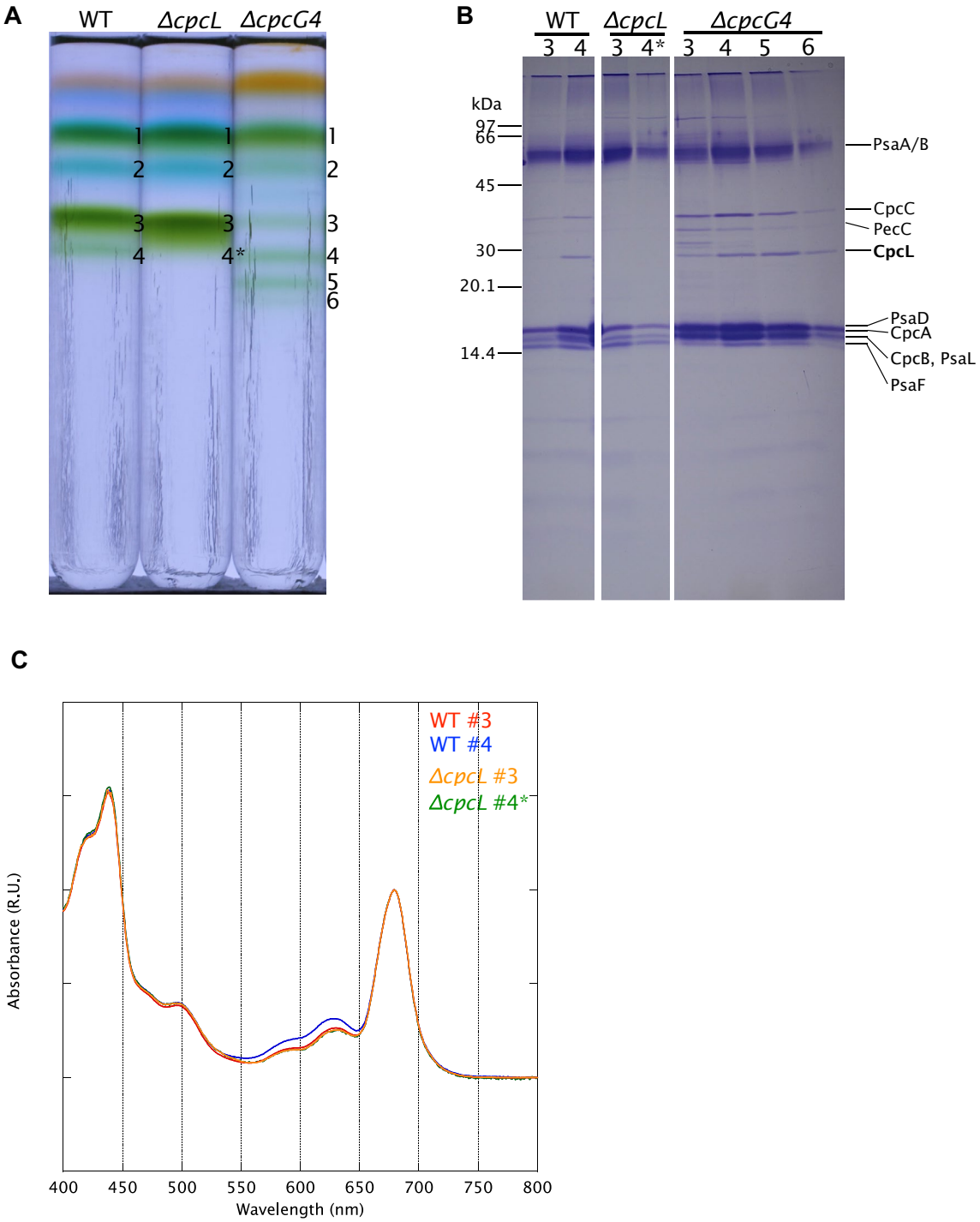

Fig. 4 Isolation of PBS-PSI supercomplexes of wild type, Δ*cpcL*, and Δ*cpcG4* mutants by centrifugation using a linear sucrose gradient. **a** Separation patterns of thylakoid membranes from wild type, Δ*cpcL*, and Δ*cpcG4* after centrifugation at 130,000×*g* for 6 h at 4 °C. **b** Coomassie staining following SDS-PAGE of the fractions. The samples of wild type fractions 3 and 4; 5.0 µg Chl*a*/lane, Δ*cpcL* fraction 3; 5.0 µg Chl*a*/lane, fraction 4; 3.4 µg Chl*a*/lane, Δ*cpcG4* fraction 3; 5.0 µg Chl*a*/lane, fraction 4; 4.3 µg Chl*a*/lane, fraction 5; 3.0 µg Chl*a*/lane, fraction 6; 1.0 µg Chl*a*/lane were loaded. Lane numbers correspond to the numbered fractions in (**a**). Bands are assigned according to a previous report based on N-terminal sequencing [9]. **c** Absorption spectra of fractions containing PSI tetramers and potential PBS-PSI supercomplexes. Fractions were directly used for the measurement without further dilution. Spectra were normalized relative to the Chl peak at 678 nm

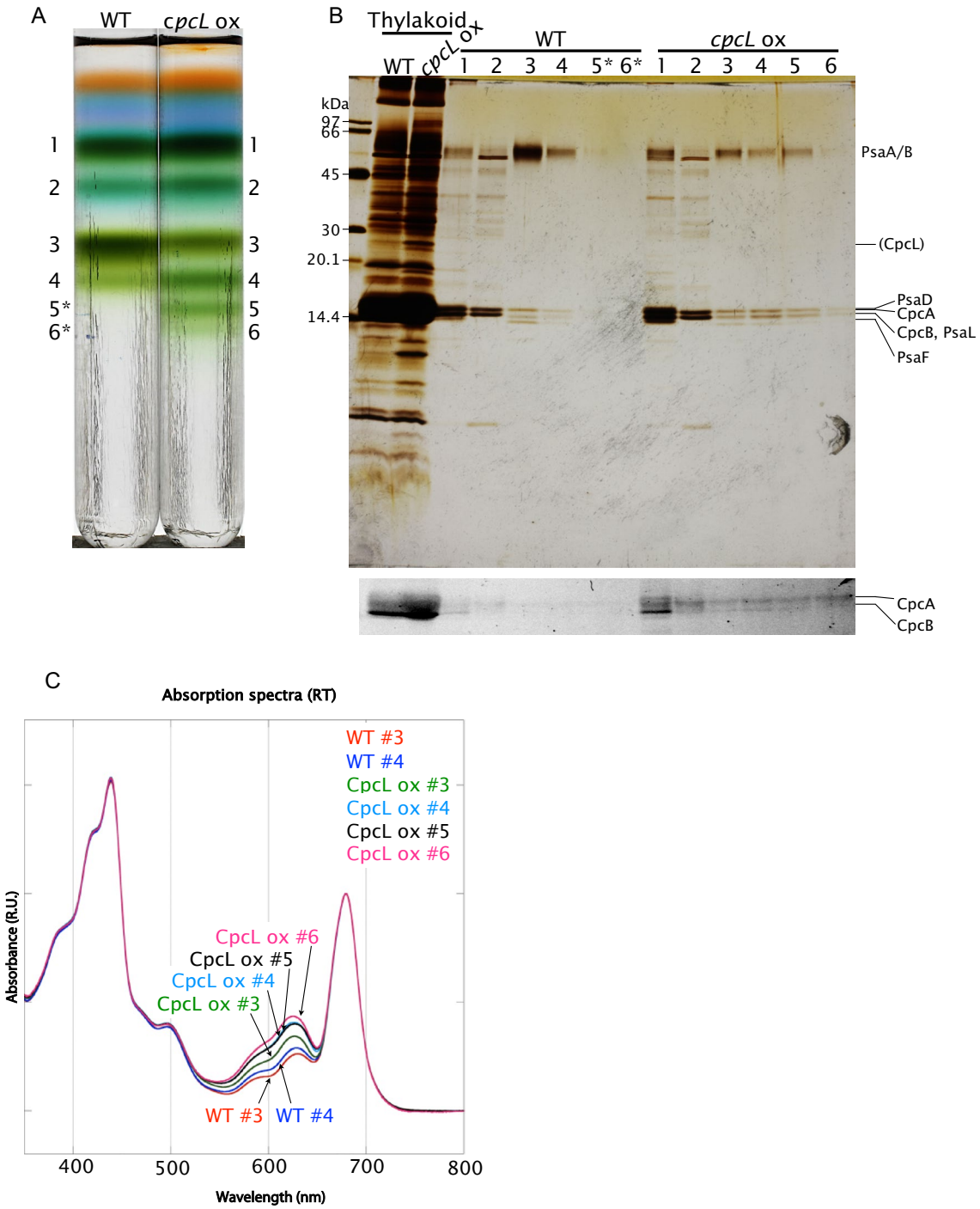

Fig. 5 Isolation of PBS-PSI supercomplexes from the wild type (WT) in comparison to the *cpcL* overexpression (*cpcL* ox) mutant by centrifugation using a linear sucrose gradient. **a** Separation patterns of thylakoid membranes from wild type and *cpcL* overexpression mutant after centrifugation at 130,000×*g* for 6 h at 4 °C. **b** Silver staining and bilin fluorescence image (lower panel) following SDS-PAGE of the protein fractions. The same volume of samples was applied to the SDS-PAGE gel. 3.3 µg Chl*a* of thylakoid membranes were loaded. Lane numbers correspond to the numbered fractions in (**a**). Bands are assigned according to a previous report based on N-terminal sequencing [9]. **c** Absorption spectra of PSI tetramer and supercomplex fractions of *cpcL* overexpression mutant. Fractions were directly used for the measurement without further dilution. Absorption spectra were normalized relative to the Chl peak at 678 nm

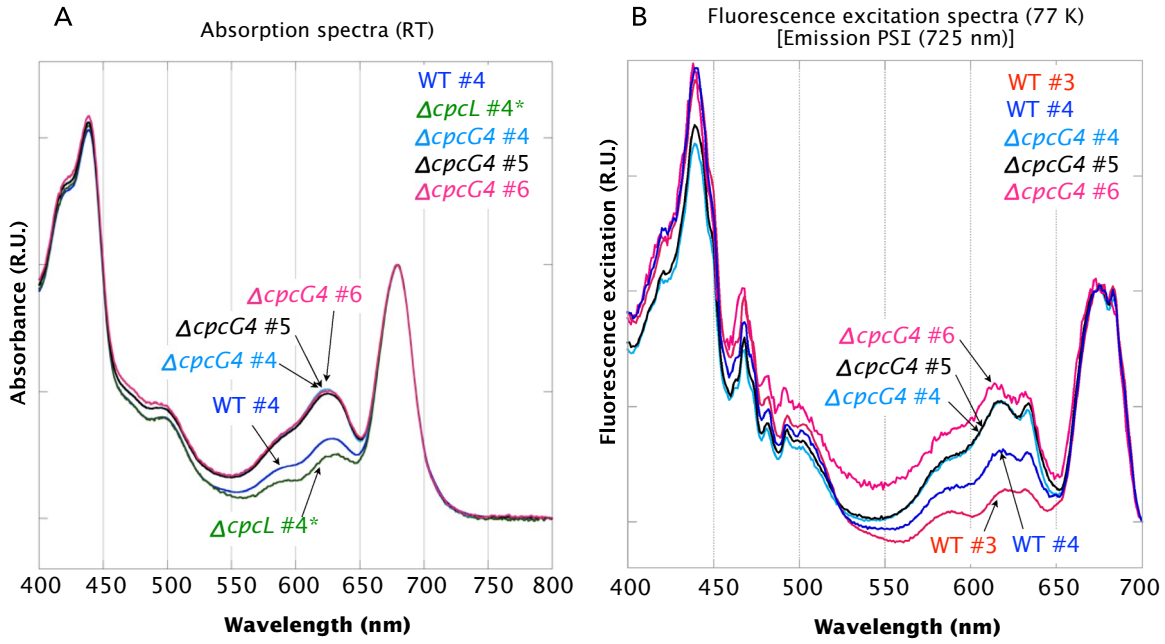

Fig. 6 Absorption and 77 K fluorescence spectra of PSI tetramer and supercomplex fractions of Δ*cpcG4* mutant. Fractions were directly used for the measurement without further dilution. **a** Absorption spectra were normalized relative to the Chl peak at 678 nm. **b** Fluorescence excitation spectra were measured to investigate the energy transfer efficiency from CpcL-PBS to PSI. The spectra were normalized relative to the Chl peak at 673 nm. PSI fluorescence was measured at 725 nm. Numbers relate to the fraction numbers of the gradients shown in Fig. 3a

The structure of *Anabaena* PSI tetramer is dimer-of-dimer, and CpcL-PBS is attached to the interface between the two monomers within the dimer [9, 12, 13]. Theoretically, the dimer-of-dimer structure revealed two such binding sites within the dimers and two potential binding sites between the dimers. According to the assumption, two more blue-green bands (fractions 5 and 6) may correspond to the second binding site within the dimer and a first binding site between the dimers.

Absorption spectra showed that the fractions 3 and 4 in *cpcL* overexpression mutant had a higher PC content than the PBS-PSI supercomplex (fraction 4) in the wild type when normalized to the Chl content (Fig. 5c, peak at 625 nm). Fractions 3 and 4 in the *cpcL* overexpression mutant correspond to the fractions 3 and 4 in the wild type and should have the same PC content. CpcL-PBSs which are present in fractions 5 and 6 may dissociate and therefore contaminate fractions 3 and 4 during ultracentrifugation. This could be the reason why the PC content in fractions 4 and 5 was similar in the *cpcL* overexpression mutant.

Our results suggest that the larger supercomplexes are PBS-PSI assemblies, which contain more CpcL-PBS, and that the *cpcL* expression level determines the amount and the PBS-to-PSI stoichiometry of this complex.

3.5 Isolation of PBS-PSI supercomplexes from the Δ*cpcG4* mutant

Further, we investigated the effect of the *cpcG4* deletion on the PBS-PSI supercomplex organization. The Δ*cpcG4* mutant showed two additional larger blue-green bands below the PBS-PSI band 4 in the sucrose gradient (Fig. 4a, fractions 5 and 6). SDS-PAGE revealed that these fractions include the subunits of PSI and the CpcL-PBS (Fig. 4b). The ratio of CpcL to PsaA/B was higher in the supercomplex fractions 5 and 6 in Δ*cpcG4* than in the PBS-PSI fraction 4 in the wild type (Fig. 4B). Absorption spectra confirmed that the supercomplex fractions 5 and 6 of Δ*cpcG4* had a higher PC-to-Chl ratio than the PBS-PSI fraction 4 of the wild type (Fig. 6a). Fractions 4–6 of Δ*cpcG4* showed almost the same absorption spectra. This may suggest a dissociation and contamination of the PC discs from the lower fractions to the upper fractions during centrifugation. Further, we measured the energy transfer from CpcL-PBS to PSI by 77 K fluorescence excitation spectroscopy (Fig. 6b). PSI fluorescence (excitation at ~ 620 nm) was increased in the supercomplex fractions 4–6 of Δ*cpcG4* compared to the PBS-PSI supercomplex in the wild type. PSI fluorescence excited around 620 nm in fraction 6 was slightly higher than in fractions 4 and 5, which showed almost identical spectra. These results suggest that the PBS-PSI supercomplexes of Δ*cpcG4* contain more CpcL-PBS than the ones from the wild type and

that these antennae are functional. These properties of the supercomplexes are very similar between Δ*cpcG4* and the *cpcL* overexpression mutant. Therefore, we suggest that not the CpcL protein levels but the CpcL/CpcG4 linker ratio determines the supercomplex assembly.

4 Discussion

A high CpcL/CpcG4 ratio in *cpcL* overexpression and Δ*cpcG4* mutants led to an increased level of PBS-PSI supercomplexes and also larger supercomplexes below the typical PBS-PSI supercomplex fraction in the sucrose gradient (Figs. 4 and 5). Our results suggest that these larger PSI supercomplexes contain more CpcL-PBS per PSI than typical PBS-PSI supercomplexes. The single particle EM structure of the PBS-PSI supercomplex revealed that CpcL-PBS is attached to the interface between two monomers within a dimer of the PSI tetramer [9]. According to the cryo-EM structure of the PSI tetramer, there are two types of monomer–monomer interfaces [12, 13]. There are two potential CpcL-PBS attachment sites within the dimers and two additional potential binding sites between dimers in the PSI tetramer. The two faster migrating bands below the PBS-PSI supercomplex band might represent PBS_2-PSI and PBS_3-PSI supercomplexes. This means that a PBS is associated with an interdimer interface in addition to the two intradimer interfaces in PBS_3-PSI supercomplexes. At the moment, we could not see a band corresponding to PBS_4-PSI supercomplexes in the gradient. This may be partly due to the disintegration of PBSs from PBS-PSI supercomplexes during the experiment. This might suggest that the fourth attachment site has only a low affinity for the binding of CpcL-PBS. Further, the bands in the sucrose gradients of fraction 6 of Δ*cpcG4* and the *cpcL* overexpression mutant were less colored than the bands of the upper PBS-PSI supercomplex bands (Figs. 4a and 5a), suggesting that the third attachment site of the PSI tetramer has also a lower affinity for CpcL-PBS. We suggest that there might be two types of interaction affinities between CpcL-PBS and the two types of monomer–monomer interfaces in the PSI tetramer. In the previously published structure of the PBS-PSI supercomplex, CpcL-PBS was attached to the monomer–monomer interface within the one PSI dimer [9]. This might suggest that the affinity of CpcL-PBS binding to the position within the dimer is higher than its affinity for binding between the dimers in the PSI tetramer. In the wild type, there were no larger supercomplexes, suggesting that the binding of one CpcL-PBS to PSI tetramer occurs preferentially. The first CpcL-PBS binding to the PSI tetramer may induce the structural changes of the PSI tetramer and reduce the binding affinity of the other three potential binding sites. Structural analysis of the supercomplexes will reveal the structural changes of the PSI tetramer by the binding of the CpcL-PBS. Overexpression of CpcL and our methods improvements, such as the use of other detergents or the use of the GraFix method [26], might have led to the recovery of more CpcL-PBS attached to the supercomplex.

77 K fluorescence excitation spectra showed a greater extent of the energy transfer from CpcL-PBS to PSI in the larger supercomplexes (Fig. 6b), suggesting that there is an increased number of functional CpcL-PBS to harvest and transduce more light energy to the PSI. Further investigations on the energy transfer from CpcL-PBS to the PSI in the supercomplexes by time-resolved fluorescence spectroscopy may reveal differences in the energy transfer efficiency between the two types of CpcL-PBS and PSI interaction in the larger supercomplexes.

Here we demonstrate that the ratio of the rod-core linker CpcG4 to the rod-membrane linker CpcL determines the assembly of the PBS-PSI supercomplexes. We previously showed that the ratio of CpcL/CpcG4 proteins is higher in heterocysts than in vegetative cells in *Anabaena* [9]. Therefore, we speculate that heterocysts may contain an increased amount of the PBS-PSI supercomplex and also PBS_2-PSI and PBS_3-PSI supercomplexes. In heterocysts, which are the specialized cells for nitrogen fixation, PSI activity is necessary to generate ATP for the nitrogenase reaction. It has been reported that CpcL is important for nitrogen fixation in *Anabaena* [13]. PBS_2-PSI and PBS_3-PSI would allow an efficient nitrogen fixation activity in heterocysts.

We could detect the PSI tetramer without CpcL-PBS binding even in the sucrose gradient of Δ*cpcG4* and *cpcL* overexpression mutants, which showed the larger PBS-PSI supercomplexes. This might suggest that the PSI tetramer without CpcL-PBS has a different function than organizing the PBS-PSI supercomplex. It is reported that PSI is assembled into a PBS-PSII-PSI supercomplex with the rod-core PBS [27]. The PSI tetramers without CpcL-PBS in the sucrose gradient might correspond to the dissociated PSI from the PBS-PSII-PSI supercomplex. This may suggest different functions of the PSI between the PBS-PSI supercomplex and the PBS-PSII-PSI supercomplex. Since PSI is involved in both the cyclic and linear electron transfer pathways, PBS-PSI supercomplex and PBS-PSII-PSI supercomplex may correspond to each function. Future physiological analysis of Δ*cpcL* and Δ*cpcG4* may reveal differences in the functions of each PBSs as a PSI antenna.

Our results suggest that CpcL and CpcG4 compete for the same rod component pool for the assembly of the two different types of PBS structures. For optimal photosynthesis under changing environmental conditions, it is necessary to regulate the expression of the two linker genes. In *Anabaena*, the *cpcL* gene is located in the *cpc* operon together with *cpcG4*. The whole *cpc* operon is transcribed from the promotor in front of *cpcB* (Fig. 2a) [28]. RNA-seq analysis

[29] suggests additional individual transcriptional start sites (TSS) for *cpcL* and the *cpcG4* genes in the *cpc* gene cluster. Further, the activity of the TSS for the *cpcG4* gene is repressed under nitrogen starvation conditions, whereas that for *cpcL* is not [29]. However, *cpcL* is also expressed under nitrogen repletion and in vegetative cells in which CpcL-PBS can function as a PSI antenna as well. Therefore, the ratio of CpcL to CpcG4 could also be important for regulating the energy transfer and linear and cyclic electron transfer pathways in vegetative cells. There may be some other conditions that increase the ratio of CpcL to CpcG4. Besides nitrogen starvation conditions, other conditions, such as high salt concentration, which require more cyclic electron transfer [30, 31], may also alter the ratio of CpcL to CpcG4 in vegetative cells.

In *Synechocystis* sp. PCC 6803, the *cpcL* gene expression is regulated by a two-component system consisting of the histidine kinase/response regulator pair, CcaS/CcaR, in a light color-dependent manner [7, 32, 33]. Green light activates autophosphorylation of the cyanobacteriochrome-type photoreceptor CcaS, and CcaS transfers a phosphate to the OmpR-type response regulator CcaR. The phosphorylated transcription factor CcaR induces *cpcL* expression. In contrast, red light converts CcaS to its ground state, and *cpcL* expression is not induced. It was reported that the PBS-PSI supercomplex level is increased under green light conditions in *Synechocystis* sp. PCC 6803 [34]. This suggests that an increased level of CpcL induces the supercomplex assembly under green light conditions in this cyanobacterium. Future work on the regulation of *cpcL* and *cpcG4* genes in *Anabaena* will clarify how the photosynthetic electron transfer is optimized by employing the two different PBS antennae under changing environmental conditions.

Supplementary Information The online version contains supplementary material available at https://doi.org/10.1007/s43630-023-00397-2.

Acknowledgements This work was supported in part by the JST CREST program (JPMJCR11B1 to M.I. and M.W.) and KAKENHI (Grant 17H05716 and 20J40231 to M.W., and 16H06558 to M.I.). The authors are grateful to Prof. Conrad W. Mullineaux for his helpful comments on this manuscript.

Funding Open Access funding enabled and organized by Projekt DEAL.

Data availability The data that support the findings of this study are available from the corresponding author, MW, upon reasonable request.

Declarations

Conflict of interest On behalf of all authors, the corresponding author states that there is no conflict of interest.

References

1. Bryant, D. A., & Canniffe, D. P. (2018). How nature designs light-harvesting antenna systems: design principles and functional realization in chlorophototrophic prokaryotes. *Journal of Physics B: Atomic, Molecular and Optical Physics, 51*, 033001. https://doi.org/10.1088/1361-6455/aa9c3c
2. Liu, L.-N., Chen, X.-L., Zhang, Y.-Z., & Zhou, B.-C. (2005). Characterization, structure and function of linker polypeptides in phycobilisomes of cyanobacteria and red algae: An overview. *Biochimica et Biophysica Acta, 1708*, 10. https://doi.org/10.1016/j.bbabio.2005.04.001
3. Watanabe, M., & Ikeuchi, M. (2013). Phycobilisome: architecture of a light-harvesting supercomplex. *Photosynthesis Research, 12*, 265–276.
4. Adir, N. (2005). Elucidation of the molecular structures of components of the phycobilisome: Reconstructing a giant. *Photosynthesis Research, 85*, 15–32. https://doi.org/10.1007/s11120-004-2143-y
5. Liu, L.-N., Chen, X.-L., Zhang, X.-Y., Zhang, Y.-Z., & Zhou, B.-C. (2005). One-step chromatography method for efficient separation and purification of R-phycoerythrin from *Polysiphonia urceolata*. *Journal of Biotechnology, 116*, 91–100. https://doi.org/10.1016/j.jbiotec.2004.09.017
6. Zheng, L., Zheng, Z., Li, X., Wang, G., Zhang, K., Wei, P., Zhao, J., & Gao, N. (2021). Structural insight into the mechanism of energy transfer in cyanobacterial phycobilisomes. *Nature Communications, 12*, 5497. https://doi.org/10.1038/s41467-021-25813-y
7. Hirose, Y., Chihong, S., Watanabe, M., Yonekawa, C., Murata, K., Ikeuchi, M., & Eki, T. (2019). Diverse chromatic acclimation processes regulating phycoerythrocyanin and rod-shaped phycobilisome in cyanobacteria. *Molecular Plant, 12*, 715–725. https://doi.org/10.1016/j.molp.2019.02.010
8. Liu, H., Weisz, D. A., Zhang, M. M., Cheng, M., Zhang, B., Zhang, H., Gerstenecker, G. S., Pakrasi, H. B., Gross, M. L., & Blankenship, R. E. (2019). Phycobilisomes harbor FNR_L in cyanobacteria. *MBio*. https://doi.org/10.1128/mBio.00669-19
9. Watanabe, M., Semchonok, D. A., Webber-Birungi, M. T., Ehira, S., Kondo, K., Narikawa, R., Fujiwara, M., Boekema, E. J., & Ikeuchi, M. (2014). Attachment of phycobilisomes in an antenna–photosystem I supercomplex of cyanobacteria. *Proceedings of the National Academy of Sciences, 111*, 2512–2517. https://doi.org/10.1073/pnas.1320599111
10. Kondo, K., Ochiai, Y., Katayama, M., & Ikeuchi, M. (2007). The Membrane-Associated CpcG2-Phycobilisome in *Synechocystis* : A New Photosystem I Antenna. *Plant Physiology, 144*, 1200–1210. https://doi.org/10.1104/pp.107.099267
11. Noji, T., Watanabe, M., Dewa, T., Itoh, S., & Ikeuchi, M. (2021). Direct energy transfer from allophycocyanin-free rod-type cpcl-phycobilisome to photosystem I. *The Journal of Physical Chemistry Letters, 6*, 6692–6697.
12. Kato, K., Nagao, R., Jiang, T.-Y., Ueno, Y., Yokono, M., Chan, S. K., Watanabe, M., Ikeuchi, M., Shen, J.-R., Akimoto, S.,

Miyazaki, N., & Akita, F. (2019). Structure of a cyanobacterial photosystem I tetramer revealed by cryo-electron microscopy. *Nature Communications, 10*, 4929. https://doi.org/10.1038/s41467-019-12942-8
13. Zheng, L., Li, Y., Li, X., Zhong, Q., Li, N., Zhang, K., Zhang, Y., Chu, H., Ma, C., Li, G., Zhao, J., & Gao, N. (2019). Structural and functional insights into the tetrameric photosystem I from heterocyst-forming cyanobacteria. *Nature Plants, 5*, 1087–1097. https://doi.org/10.1038/s41477-019-0525-6
14. Rippka, R. (1988). Isolation and purification of cyanobacteria. In: Methods Enzymol. Elsevier, pp. 3–27. https://doi.org/10.1016/0076-6879(88)67004-2.
15. Black, T. A., Cai, Y., & Wolk, C. P. (1993). Spatial expression and autoregulation of hetR, a gene involved in the control of heterocyst development in *Anabaena*. *Molecular Microbiology, 9*, 77–84. https://doi.org/10.1111/j.1365-2958.1993.tb01670.x
16. Wei, T.-F., Ramasubramanian, T. S., & Golden, J. W. (1994). *Anabaena* sp. strain PCC 7120 ntcA gene required for growth on nitrate and heterocyst development. *Journal of Bacteriology, 176*, 4473–4482. https://doi.org/10.1128/jb.176.15.4473-4482.1994
17. Yoon, H.-S., & Golden, J. W. (1998). Heterocyst pattern formation controlled by a diffusible peptide. *Science, 282*, 935–938. https://doi.org/10.1126/science.282.5390.935
18. Huang, H.-H., & Lindblad, P. (2013). Wide-dynamic-range promoters engineered for cyanobacteria. *Journal of Biological Engineering, 7*, 10. https://doi.org/10.1186/1754-1611-7-10
19. Huang, H.-H., Camsund, D., Lindblad, P., & Heidorn, T. (2010). Design and characterization of molecular tools for a Synthetic Biology approach towards developing cyanobacterial biotechnology. *Nucleic Acids Research, 38*, 2577–2593. https://doi.org/10.1093/nar/gkq164
20. Olmedo-Verd, E., Flores, E., Herrero, A., & Muro-Pastor, A. M. (2005). HetR-dependent and -independent expression of heterocyst-related genes in an *Anabaena* strain overproducing the NtcA transcription factor. *Journal of Bacteriology, 187*, 1985–1991. https://doi.org/10.1128/JB.187.6.1985-1991.2005
21. Elhai, J., & Wolk, C. P. (1990). Developmental regulation and spatial pattern of expression of the structural genes for nitrogenase in the cyanobacterium *Anabaena*. *EMBO Journal, 9*, 3379–3388. https://doi.org/10.1002/j.1460-2075.1990.tb07539.x
22. Cai, Y., & Wolk, C. P. (1990). Use of a conditionally lethal gene in *Anabaena* sp. strain PCC 7120 to select for double recombinants and to entrap insertion sequences. *Journal of Bacteriology, 172*, 3138–3145. https://doi.org/10.1128/jb.172.6.3138-3145.1990
23. Ikeuchi, M., & Inoue, Y. (1988). Partial characterization of the iodination site in D1 protein of manganese-retaining and manganese-depleted photosystem II membranes. *Plant and Cell Physiology, 29*, 695–705. https://doi.org/10.1093/oxfordjournals.pcp.a077549
24. Aro, E.-M., Suorsa, M., Rokka, A., Allahverdiyeva, Y., Paakkarinen, V., Saleem, A., Battchikova, N., & Rintamäki, E. (2005). Dynamics of photosystem II: A proteomic approach to thylakoid protein complexes. *Journal of Experimental Botany, 56*, 347–356. https://doi.org/10.1093/jxb/eri041
25. Chang, L., Liu, X., Li, Y., Liu, C.-C., Yang, F., Zhao, J., & Sui, S.-F. (2015). Structural organization of an intact phycobilisome and its association with photosystem II. *Cell Research, 25*, 726–737. https://doi.org/10.1038/cr.2015.59
26. Kastner, B., Fischer, N., Golas, M. M., Sander, B., Dube, P., Boehringer, D., Hartmuth, K., Deckert, J., Hauer, F., Wolf, E., Uchtenhagen, H., Urlaub, H., Herzog, F., Peters, J. M., Poerschke, D., Lührmann, R., & Stark, H. (2008). GraFix: Sample preparation for single-particle electron cryomicroscopy. *Nature Methods, 5*, 53–55. https://doi.org/10.1038/nmeth1139
27. Liu, H., Zhang, H., Niedzwiedzki, D. M., Prado, M., He, G., Gross, M. L., & Blankenship, R. E. (2013). Phycobilisomes supply excitations to both photosystems in a megacomplex in cyanobacteria. *Science, 342*, 1104–1107. https://doi.org/10.1126/science.1242321
28. Bryant, D. A., Stirewalt, V. L., Glauser, M., Frank, G., Sidler, W., & Zuber, H. (1991). A small multigene family encodes the rod-core linker polypeptides of *Anabaena* sp. PCC7120 phycobilisomes. *Gene, 107*, 91–99. https://doi.org/10.1016/0378-1119(91)90301-Q
29. Mitschke, J., Vioque, A., Haas, F., Hess, W. R., & Muro-Pastor, A. M. (2011). Dynamics of transcriptional start site selection during nitrogen stress-induced cell differentiation in *Anabaena* sp. PCC7120. *Proceedings of the National Academy of Sciences, 108*, 20130–20135. https://doi.org/10.1073/pnas.1112724108
30. Jeanjean, R., Bédu, S., Havaux, M., Matthijs, H. C. P., & Joset, F. (1998). Salt-induced photosystem I cyclic electron transfer restores growth on low inorganic carbon in a type 1 NAD(P)H dehydrogenase deficient mutant of *Synechocystis* PCC6803. *FEMS Microbiology Letters, 167*, 131–137. https://doi.org/10.1111/j.1574-6968.1998.tb13218.x
31. Hagemann, M., Jeanjean, R., Fulda, S., Havaux, M., Joset, F., & Erdmann, N. (1999). Flavodoxin accumulation contributes to enhanced cyclic electron flow around photosystem I in salt-stressed cells of *Synechocystis* sp. strain PCC 6803. *Physiologia Plantarum, 105*, 670–678. https://doi.org/10.1034/j.1399-3054.1999.105411.x
32. Hirose, Y., Narikawa, R., Katayama, M., & Ikeuchi, M. (2010). Cyanobacteriochrome CcaS regulates phycoerythrin accumulation in *Nostoc punctiforme*, a group II chromatic adapter. *Proceedings of the National Academy of Sciences, 107*, 8854–8859. https://doi.org/10.1073/pnas.1000177107
33. Hirose, Y., Shimada, T., Narikawa, R., Katayama, M., & Ikeuchi, M. (2008). Cyanobacteriochrome CcaS is the green light receptor that induces the expression of phycobilisome linker protein. *Proceedings of the National Academy of Sciences, 105*, 9528–9533. https://doi.org/10.1073/pnas.0801826105
34. Gao, F., Ogawa, T., & Ma, W. (2018). Effect of green light on the amount and activity of NDH-1-PSI supercomplex in *Synechocystis* sp. strain PCC 6803. *Photosynthetica, 56*, 316–321. https://doi.org/10.1007/s11099-018-0790-z